Mesoporous Thin-Film on Highly-Sensitive Resonant Chemical Sensor for Relative Humidity and CO2 Detection

ARTICLE *in* ANALYTICAL CHEMISTRY · FEBRUARY 2012

Impact Factor: 5.64 · DOI: 10.1021/ac300225c · Source: PubMed

5 AUTHORS, INCLUDING:

Hyunjoo J Lee
Stanford University
47 PUBLICATIONS **330** CITATIONS
SEE PROFILE

Kwan Kyu Park
Hanyang University
57 PUBLICATIONS **396** CITATIONS
SEE PROFILE

Pierre T Khuri-Yakub
Stanford University
571 PUBLICATIONS **8,811** CITATIONS
SEE PROFILE

analytical chemistry

Letter

pubs.acs.org/ac

Mesoporous Thin-Film on Highly-Sensitive Resonant Chemical Sensor for Relative Humidity and CO_2 Detection

Hyunjoo J. Lee,*[,†] Kwan Kyu Park,[†] Mario Kupnik,[§] Nicholas A. Melosh,[‡] and Butrus T. Khuri-Yakub[†]

[†]Edward L. Ginzton Laboratory, Stanford University, Stanford, California 94305, United States

[‡]Materials Science & Engineering, Stanford University, Stanford, California 94305, United States

[§]Brandenburg University of Technology, 03046 Cottbus, Germany

Supporting Information

ABSTRACT: Distributed sensing of gas-phase chemicals is a promising application for mesoporous materials when combined with highly sensitive miniaturized gas sensors. We present a direct application of a mesoporous silica thin film on a highly sensitive miniaturized resonant chemical sensor with a mass sensitivity at the zeptogram scale for relative humidity and CO_2 detection. Using mesoporous silica thin-film, we report one of the lowest volume resolutions and a sensitive detection of 5.1×10^{-4}% RH/Hz to water vapor in N_2, which is 70 times higher than a device with a nontemplated silica layer. In addition, a mesoporous thin-film that is functionalized with an amino-group is directly applied on the resonant sensor, which exhibits a volume sensitivity of 1.6×10^{-4}%/Hz and a volume resolution of 1.82×10^{-4}% to CO_2 in N_2.

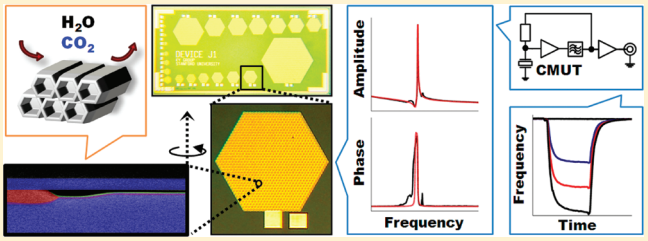

Portable chemical sensors enabled through microtechnology offer distinctive advantages over the existing benchtop chemical analyzers, including small size, low cost, low power, and complementary metal-oxide semiconductor (CMOS) compatibility. These miniaturized chemical sensors play important roles in a wide range of emerging applications, such as environment monitoring, homeland security, and medical home care applications. For example, monitoring air quality and climate change using distributed sensors is vital for attaining environment sustainability.

For these field-based portable chemical sensors, achieving high sensitivities to the analytes of interest is critical because of unpredictable changes in both the environment and interference chemicals. Higher sensitivity can be achieved by optimizing either the performance of the physical sensor or the chemical functionalization layer. Physical sensors are often based on different parameters, such as mass,[1] capacitance,[2] resistance,[3] or deflection.[4] Among these, resonant sensors based on mass-loading have demonstrated high sensitivity and volume resolution due to high noise immunity from high-Q resonance and wide dynamic range.[5] Resonant chemical detectors based on microelectromechanical systems (MEMS) include capacitive micromachined ultrasonic transducers (CMUTs),[1] micro/nanocantilevers,[6] film bulk acoustic resonators (FBAR),[7] and surface acoustic resonators.[8]

One method of enhancing the sensitivity of a given physical sensor is to increase the surface-to-volume ratio of the layer that reacts with the analyte by depositing materials such as carbon nanotubes (CNTs),[9] graphene,[10] or mesoporous powders.[11] Among these, mesoporous materials have several advantages, such as regularity, repeatability in deposition, and synthesis temperatures that are compatible with the thermal budget of CMOS processing (<400 °C). In addition, compared to depositing conglomerates of mesoporous powders, depositing a continuous and uniform thin film of the mesoporous materials directly on the resonant sensor through self-assembly helps control the loading condition of the resonant device.[12−14]

In this Letter, we present the successful application of a continuous mesoporous silica thin film directly on CMUTs. The goal was to implement a highly sensitive resonant sensor with improved volume sensitivity for relative humidity and CO_2 detection. The applied thin-films were first characterized through high resolution scanning electron microscopy (HRSEM) and small-angle X-ray diffraction (SAXRD). Chemical reaction of these films to water vapors and CO_2 were then examined using the CMUT resonant sensor as the physical sensor platform.

For humidity detection, thermally stable continuous SBA-15 mesoporous silica films were directly grown on top of the sensor. A synthesis method developed by Zhao et al.,[15] which is suitable for dip-coating based on evaporation-induced self-assembly (EISA), was used [see the Synthesis Section I in the Supporting Information]. For CO_2 detection, aminopropyl-functionalized mesoporous silica thin-film was directly grown using the one-pot synthesis developed by Zhang et al.[16] to induce chemisorption between amine sites and carbon dioxide. (3-Aminopropyl) triethoxysilane (APTES) was used to provide the amino sites (Synthesis Section II in Supporting Information).[17] Samples

Received: January 22, 2012
Accepted: February 27, 2012

   dx.doi.org/10.1021/ac300225c | *Anal. Chem.* XXXX, XXX, XXX−XXX

prepared with different synthesis parameters are summarized in Table 1 (Table S1 in Supporting Information).

Table 1. Summary of the Prepared CMUT Resonant Sensors with Various Mesoporous Layers

sample	functionalization layer	mesophase
I	sputtered oxide	none
II	nontemplated oxide	none
III	mesoporous silica	3D ($P6_3/mmc$)
IV	mesoporous silica	2D ($p6mm$)
V	APTES functionalized mesoporous silica	2D ($p6mm$)

HRSEM and SAXRD were used to estimate pore-size, morphology, film thickness, and ordering of pore structures of the applied thin films. For Sample IV, HRSEM images were obtained on an ebeam lithography system (Raith 150 Ebeam Writer), equipped with HRSEM inspection, operating at an acceleration voltage of 10 kV. The HRSEM image of the film in the top view shows striations on a 14 nm length scale (mesochannels) aligned along the dip-coating direction (Figure 1a).

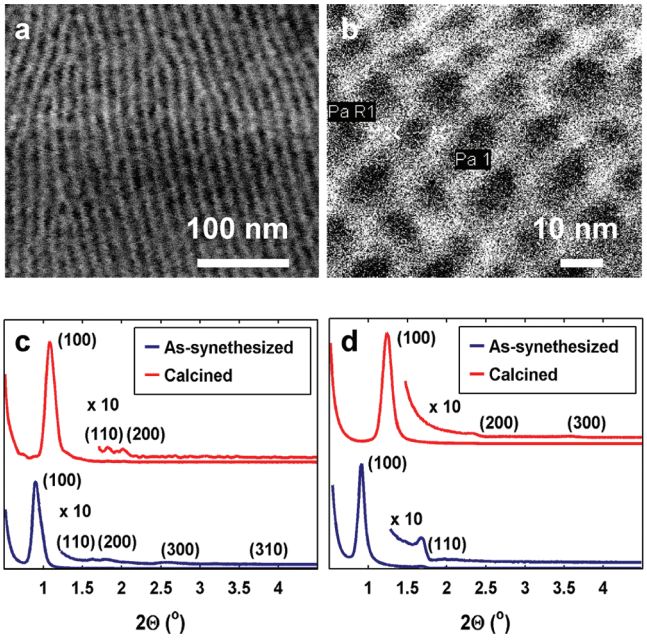

Figure 1. HRSEM images of as-deposited 2D hexagonal mesostructured silica thin film ($p6mm$) in (a) top and (b) close-up cross-sectional. SAXRD patterns of (c) as-deposited and calcined 2D hexagonal ($p6mm$) and (d) as-deposited and calcined 3D hexagonal ($P63/mmc$) mesoporous silica film, measured using an X-ray diffraction system (PANalytical X'Pert PRO) using Cu K radiation.

In addition, the cross-sectional view demonstrates that the layers of mesochannels were oriented parallel to the substrate, where the number of layers depended on the dip-coating parameters, such as the coating solution concentration and the dip-coating rate. The close-up cross-section view shows that pores are packed in 2D plane $p6mm$ hexagonal symmetry with a pore size on the order of ~11 nm (Figure 1b).

The SAXRD patterns were obtained by an X-ray diffraction system (PANalytical X'Pert PRO) using Cu K radiation (45 kV, 40 mV) on both 2D ($p6mm$) and 3D ($P6_3/mmc$) hexagonal mesoporous silica films. Five XRD peaks (Figure. 1c) were observed on Sample IV, which can be indexed as (100), (110), (200), (300), and (310) reflections of a highly ordered hexagonal ($p6mm$) structure with a large unit cell (a = 112.8 Å). Three peaks (Figure 1d) indexed with (100), (110), and (200) were observed on the as-deposited 3D hexagonal structure with a = 112.5 Å. The XRD pattern of the calcined film showed that the oriented $P6_3/mmc$ mesostructure was preserved and that the film was thermally stable. Due to the removal of surfactant, the XRD peaks appeared at a slightly larger angle after calcination, which translated to a reduced pore size of a = 82 Å.

We then studied the viability of these films for relative humidity and CO_2 detection using the highly sensitive CMUT resonant sensors. In total, 22 CMUT resonant sensors were fabricated on a 2.5 mm-by-5 mm die (Figure 2b). A single CMUT resonant sensor is typically composed of hundreds to thousands of circular capacitive resonators, all electrically connected in parallel through the top electrode (Figure 2d).

The individual resonant structure is a capacitor with a 500 nm thick highly doped single-crystal silicon plate as the top electrode and a conductive substrate as the bottom electrode (Figure 2c). These two electrodes are separated by a 40 nm thin evacuated cavity, which allows this multiresonator CMUT sensor to achieve a relatively high quality factor of ~300−500 in air despite massive parallelism. When the CMUT resonator is biased at a DC bias voltage of 48 V and an AC amplitude of 50 mV_{rms}, the electrical input impedance shows the parallel resonance at 47.4 MHz with a quality factor of 240 (Figure 2e). Because of this high quality factor for a given actuation area, CMUTs can be designed with a larger active area compared to other types of resonant sensors such as nanocantilevers.[18] The individual resonant structure with a radius of 5.3 μm has an effective mass of 103 fg and a fundamental mechanical resonant frequency of approximately 50 MHz, resulting in a high mass sensitivity of 48.8 zg/Hz/μm^2. We employed a free-running oscillator to track changes in the CMUT resonant frequency due to absorption of target vapor species in real-time (Figure 2f,g). Details of the CMUT fabrication and structure, transduction mechanism, and the interface circuits have been described previously.[1,19]

The loading effect of applying a mesostructure thin film on the CMUT was characterized by measuring the input impedance before the coating, after the coating (as-deposited), and after the calcination (Figure S1 in Supporting Information). For a circular resonant plate, the resonant frequency of the fundamental mode is inversely proportional to the effective mass, as shown below:[20]

$$f_0 = \frac{0.83}{a}\sqrt{\frac{Et^3}{m(1-\nu^2)}} \quad (1)$$

where a is the radius, E is the Young's modulus, t is the thickness, ν is the Poisson ratio, and m is the mass of the circular plate. Consequently, the resonant frequency of the CMUT coated with the as-deposited silica film was lower than the initial frequency due to the mass-loading. When the surfactant was removed from the film through the calcination, the resonant frequency increased again, but this frequency was not as high as the initial frequency due to the remaining mesoporous structures, as predicted in (1).

Chemical experiments were performed on the prepared CMUT samples to study the mesoporous silica film as a functionalization layer for the resonant sensor using a chemical setup based on the saturation bubbler method (Figure S2 in Supporting Information). First, to evaluate the effectiveness of mesoporous silica film as a functionalization layer for humidity detection, three samples

dx.doi.org/10.1021/ac300225c | Anal. Chem. XXXX, XXX, XXX−XXX

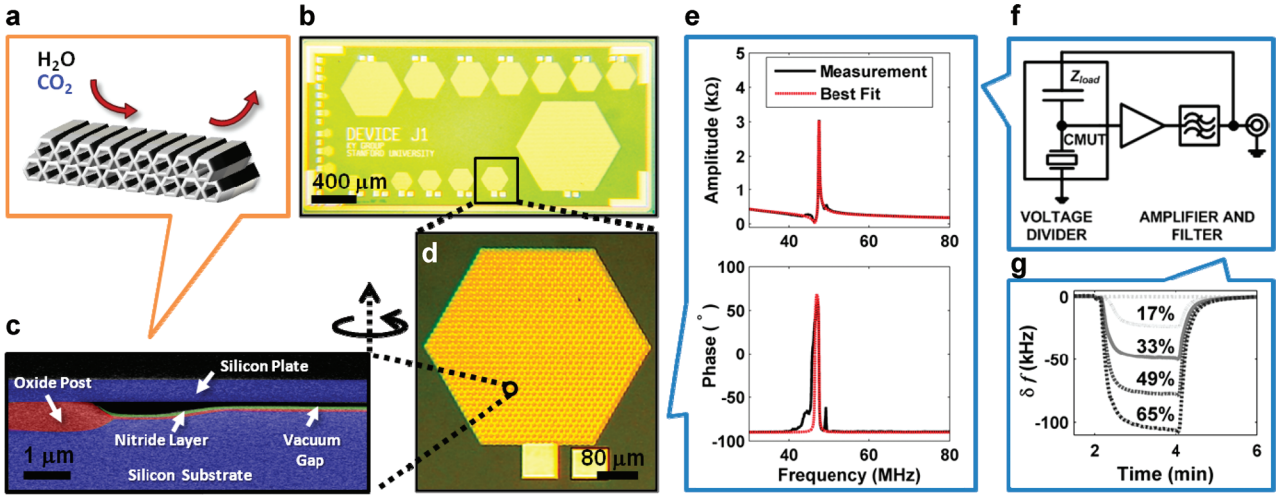

Figure 2. (a) Illustration of mesoporous silica thin film. (b) Optical picture of a single die, showing an array of multiple elements. (c) Scanning electron microscope (SEM) image of the cross-section of a single CMUT resonator. (d) Optical picture of a single element with 1027 cells. (e) Plot of measured and fitted electrical impedance characteristics of the CMUT resonator biased at 48 V. (f) Block diagram of the free-running oscillator for real-time measurements. (g) Transient frequency shifts in response to various concentrations of water vapors in N_2. Humidity vapor starts to flow in at 120 s and stops after 240 s.

were prepared; Samples I, II, and III were coated with a 50 nm sputtered oxide layer without any template (reference sample), an approximately 150 nm silica layer with no template, and an approximately 85 nm 3D mesoporous silica layer, respectively. The silica layer on the Sample II was formed without the triblock copolymer in the final mixture. We measured the transient frequency shifts to various relative humidity (RH) levels from 0% to 80% in 16% increments in N_2. To illustrate, the transient frequency shifts of three samples to 65% RH are shown (Figure 3a). Compared to Sample I with sputtered oxide, large increases in the frequency shifts (~60 times and ~80 times, respectively) are observed from Samples III and IV with mesoporous silica layers.

The volume sensitivity to water vapors is extrapolated first by estimating the slope of the maximum frequency shifts against various concentrations using the best-fit linear regression and then computing the inverse of the estimated slope (Figure 3b). The CMUT coated with the mesoporous silica layer (Sample IV) exhibited a volume sensitivity to relative humidity that is approximately 7.5 and 70 times larger than that of the CMUTs coated with the sputtered oxide (Sample I) and the nontemplated oxide (Sample II), respectively. The non-templated silica layer exhibited an order of magnitude increase in sensitivity compared to the sputtered oxide layer because of the remaining oxygen–hydrogen (−OH) bonds from the sol–gel solution. The sensitivity of the mesoporous layers with two different phase morphologies was also investigated: 2D (*p6mm*) and 3D ($P6_3/mmc$) hexagonal structures. The two samples did not show a significant difference in sensitivity (Figure 3b).

Short-term frequency stability measurements in the time domain, expressed as an overlapped Allan deviation,[21] were used to estimate the noise Δf of the system and, thus, the limit of detection (LOD) of a mass-loading-based resonant sensor. An Allan deviation is a square root of two-sample variance computed between successive frequency samples measured without dead-time over a sampling period and is defined as:[21]

$$\sigma_y(\tau) = \sqrt{\frac{1}{2(M-1)} \sum_{i=1}^{M-1} (y_{i+1} - y_i)^2} \qquad (2)$$

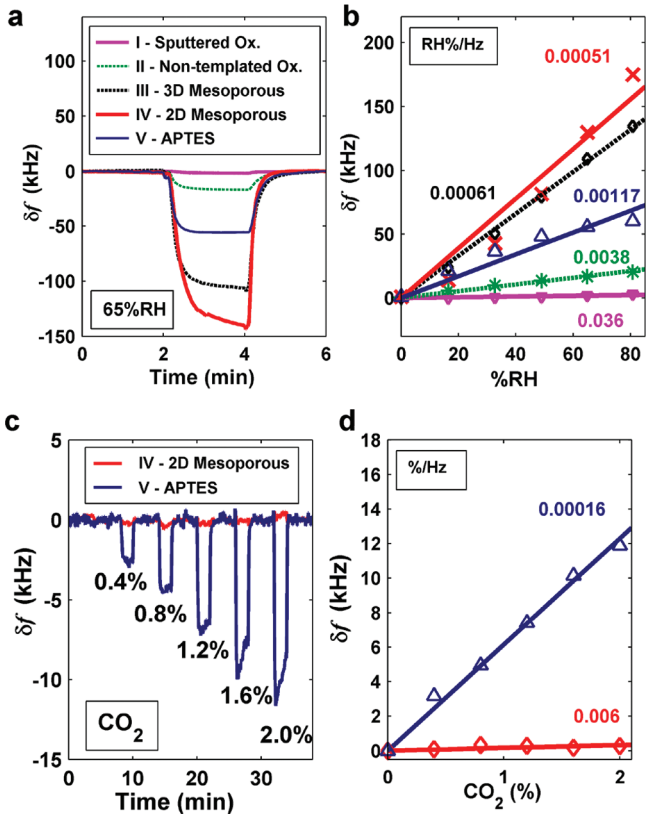

Figure 3. (a) Transient frequency shifts of Samples I, II, III, IV, and V in response to 65% RH in N_2. Water vapor starts to flow at 120 s and stops at 480 s. (b) Plot of maximum frequency shifts observed at different RH values for Samples I, II, III, IV, and V. (c) Transient frequency shifts of Samples IV and V in response to various concentrations of CO_2 in N_2, which starts to flow in at 2 min and stops at 4 min. (d) Plot of maximum frequency shifts observed at different CO_2 concentrations for Samples IV and V.

where M is number of frequency samples and y is fractional frequency. An Allan deviation can be also derived analytically from phase noise and thus is a function of Q, f_0, thermal noise,

dx.doi.org/10.1021/ac300225c | Anal. Chem. XXXX, XXX, XXX−XXX

and power of the oscillation signal. The lowest overlapped Allan deviation measured for the oscillator based on the CMUT sensors with 2D mesoporous silica thin-film (Sample IV) was 0.90 Hz (1σ), at an averaging time of 100 ms (Figure S3 in Supporting Information). Thus, the volume resolution of Sample IV to water vapors is 1.4×10^{-3}% RH (3σ), which is one of the lowest reported in the literature (Figure S4 in Supporting Information).

For CO_2 detection, mesoporous silica layer functionalized with APTES (Sample V) was self-assembled on top of the CMUT sensor. The sensor exhibited a volume sensitivity of 1.6×10^{-4}%/Hz to CO_2 in dry N_2, which was ~38 times larger than that of Sample IV (Figure 3c,d). The lowest overlapped Allan deviation of the oscillator based on Sample V was 0.38 Hz (1σ) at an averaging time of 150 ms (Figure S4 in Supporting Information), which resulted in a volume resolution of 1.82×10^{-4}% to CO_2 (3σ). Given that the ambient CO_2 concentration in air is 0.03%, this sensor provides a more than sufficient resolution and sensitivity to track CO_2 concentration.

Mesoporous materials with a pore size between 2 and 50 nm are known to exhibit an adsorption hysteresis due to capillary condensation.[22] To examine the hysteresis characteristics, we exposed Samples VI and V to various humidity and CO_2 concentrations, respectively, from low to high for absorption and then high to low for desorption. Both samples exhibit a hysteresis characteristic where sensitivity is slightly smaller at the desorption (Figure 4). In the controlled experimental settings, the hysteresis

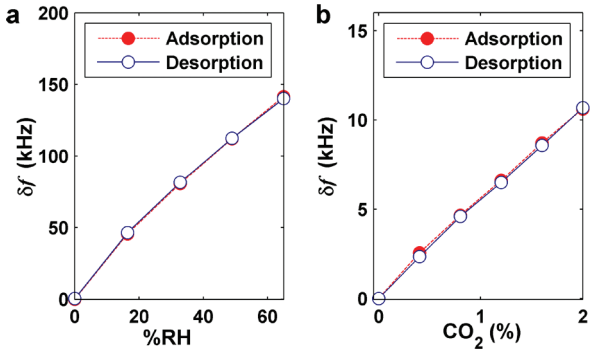

Figure 4. Hysteresis (adsorption/desorption) curves of (a) Sample IV for RH detection and (b) Sample V for CO_2 detection.

characteristics can be recorded and compensated for through an external signal processing unit that stores the previous values.

We have presented a promising CMUT-based sensor for relative humidity and CO_2 detection using mesoporous silica as a chemical functionalization layer. Amino-functionalized and plain mesoporous silica thin-films were successfully applied on the resonant sensors using the convenient co-condensation (one-pot) sol–gel self-assembly, which provided a uniform layer suitable for resonant sensors. Using the mesoporous silica thin-film on the highly sensitive chemical sensor system, more than an order of magnitude improvement in the volume sensitivity (5.1×10^{-4}% RH/Hz) was achieved. Based on low frequency noise, the presented sensors also showed an excellent volume resolution of 1.4×10^{-3}% RH (3σ). In addition, the sensor coated with amino-functionalized mesoporous layer exhibited a volume sensitivity of 1.6×10^{-4}%/Hz and a volume resolution of 1.82×10^{-4}% to CO_2. Investigating the cross-sensitivity, achieving the selectivity through the array implementation, and testing the reproducibility of the layer deposition will be part of our future work.

■ ASSOCIATED CONTENT

Supporting Information

Additional information as noted in text. This material is available free of charge via the Internet at http://pubs.acs.org.

■ AUTHOR INFORMATION

Corresponding Author

*E-mail: hyunjoo@stanford.edu.

Notes

The authors declare no competing financial interest.

■ ACKNOWLEDGMENTS

We thank Defense Advanced Research Projects Agency, Microsystems Technology Office for their financial support of this project through grant N66001-06-1-2030.

■ REFERENCES

(1) Lee, H. J.; Park, K. K.; Kupnik, M.; Oralkan, Ö.; Khuri-Yakub, B. T. *Anal. Chem.* **2011**, *83* (24), 9314–9320.
(2) Snow, E. S.; Perkins, F. K.; Houser, E. J.; Badescu, S. C.; Reinecke, T. L. *Science* **2005**, *307*, 1942.
(3) Innocenzi, P.; Falcaro, P.; Bertolo, J. M.; Bearzotti, A.; Amenitsch, H. *J. Non-Cryst. Solids* **2005**, *351*, 1980–1986.
(4) Voiculescu, I.; Zaghloul, M. E.; McGill, R. A.; Houser, E. J.; Fedder, G. K. *IEEE Sens. J.* **2005**, *5* (4), 641–647.
(5) Kirianaki, N. V.; Yurish, S. Y.; Shpak, N. O.; Deynega, V. P. *Data acquisition and signal processing for smart sensors*, 1st ed.; Wiley: New York, 2002.
(6) Thundat, T.; Chen, G. Y.; Warmack, R. J.; Allison, D. P.; Wachter, E. A. *Anal. Chem.* **1995**, *67*, 519–521.
(7) Gabl, R.; Green, E.; Schrelter, M.; Feucht, H. D.; Zelninger, H.; Primg, R.; Pitzer, D.; Eckstein, G.; Wersing, W.; Reichl, W.; Runck, J. *Second IEEE International Conference on Sensors*. Toronto, Canada, Oct. 22–24, 2003.
(8) Penza, M.; Cassano, G. *Sens. Actuators, B* **2000**, *68* (1–3), 300–306.
(9) Chen, H. W.; Wu, R. J.; Chan, K. H.; Sun, Y. L.; Su, P. G. *Sens. Actuators B* **2005**, *104* (1), 80–84.
(10) Dan, Y.; Lu, Y.; Kybert, N. J.; Luo, Z.; Johnson, A. T. C. *Nano Lett.* **2009**, *9* (4), 1472–1475.
(11) Xu, P.; Yu, H.; Li, X. *Anal. Chem.* **2011**, *83* (9), 3448–3454.
(12) Yu, H. T.; Xu, P. C.; Xu, T. G.; Li, X. *2011 IEEE 24th International Conference on Micro Electro Mechanical Systems (MEMS)*. Cancun, Mexico, Jan. 23–27, 2011.
(13) Palaniappan, A.; Xiaodi, S.; Tay, F. E. H. *IEEE Sens. J.* **2006**, *6* (6), 1676–1682.
(14) Yuliarto, B.; Zhou, H.; Yamada, T.; Honma, I.; Katsumura, Y.; Ichihara, M. *Anal. Chem.* **2004**, *76* (22), 6719–6726.
(15) Zhao, D.; Yang, P.; Melosh, N.; Feng, J.; Chmelka, B. F.; Stucky, G. D. *Adv. Mater.* **1998**, *10* (16), 1380–1385.
(16) Zhang, X.; Wang, J.; Wenjian, W.; Liu, C.; Qian, S. *J. Sol-Gel Sci. Technol.* **2007**, *43* (3), 305–311.
(17) Zhou, R.; Schmeisser, D.; Gopel, W. *Sens. Actuators, B* **1996**, *33* (1–3), 188–193.
(18) Li, M.; Myrs, E. B.; Tang, H. X.; Aldridge, S. J.; McCaig, H. C.; Whiting, J. H.; Simonson, R. J.; Lewis, N. S.; Roukes, M. L. *Nano Lett.* **2010**, *10* (10), 3899–3903.
(19) Park, K. K.; Lee, H. J.; Kupnik, M.; Khuri-Yakub, B. T. *J. Microelectromech. Syst.* **2011**, *20* (2), 95–103.
(20) Meirovitch, L. *Analytical Methods in Vibrations*, 1st ed.; Macmillan: New York, 1967.
(21) Allan, D. *IEEE Trans. Ultrason., Ferroelectr., Freq. Control* **1987**, *34* (6), 647–654.
(22) Ciesla, U; Schüth, F *Microporous Mesoporous Mater.* **1999**, *27* (2–3), 131–149.